

CCS and NH₃ emission associated with low-mass young stellar objects

Itziar de Gregorio-Monsalvo¹, José F. Gómez^{1,2}, Olga Suárez¹, Thomas B. H. Kuiper³, Luis F. Rodríguez⁴, Elena Jiménez-Bailón⁵

ABSTRACT

In this work we present a sensitive and systematic single-dish survey of CCS emission (complemented with ammonia observations) at 1 cm, toward a sample of low- and intermediate-mass young star forming regions known to harbor water maser emission, made with NASA’s 70 m antenna at Robledo de Chavela, Spain. Out of the 40 star forming regions surveyed in the CCS(2₁–1₀) line, only 6 low-mass sources show CCS emission: one transitional object between pre-stellar and protostellar Class 0 phase (GF9-2), three Class 0 protostars (L1448-IRS3, L1448C, and B1-IRS), a Class I source (L1251A), and a young T Tauri star (NGC2071-North). Since CCS is considered an “early-time” ($\lesssim 10^5$ yr) molecule, we explain these results by either proposing a revision of the classification of the age of NGC2071-North and L1251A, or suggesting the possibility that the particular physical conditions and processes of each source affect the destruction/production of the CCS. No statistically significant relationship was found between the presence of CCS and parameters of the molecular outflows and their driving sources. Nevertheless, we found a significant relationship between the detectability of CCS and the ammonia peak intensity (higher in regions with CCS), but not with its integrated intensity. This tendency found may suggest that the narrower ammonia line widths in the less turbulent medium associated

¹Laboratorio de Astrofísica Espacial y Física Fundamental (INTA), Apartado 50727, E-28080 Madrid, Spain

²Instituto de Astrofísica de Andalucía (CSIC), Apartado 3004, E-18080 Granada, Spain

³Jet Propulsion Laboratory, California Institute of Technology, USA

⁴Centro de Radioastronomía y Astrofísica, UNAM, Apartado Postal 3-72 (Xangari), 58089 Morelia, Michoacán. Mexico

⁵XMM-Newton Science Operation Center/RSSD-ESA, Apartado 50727, E-28080 Madrid, Spain.

with younger cores may compensate for the differences in ammonia peak intensity, rendering differences in integrated intensity negligible. From the CCS detection rate we derive a lifetime of this molecule of $\simeq (0.7-3)\times 10^4$ yr in low-mass star forming regions.

Subject headings: Stars: formation, pre-main sequence— ISM: clouds, evolution, molecules.

–

1. Introduction

The lines of the CCS molecule are a powerful tool for studying the physical conditions and the structure of dark molecular clouds, because they are intense, abundant and not very opaque in these regions. In addition, CCS is very useful for performing dynamical studies, since it is heavier than other high density gas tracers and it has no hyperfine structure (Saito et al. 1987; Suzuki et al. 1992).

Moreover, CCS is useful for obtaining information about the age of molecular clouds. Previous single-dish observations show that CCS lines are intense in starless, cold, quiescent cores, while ammonia tends to be abundant in star forming regions (Suzuki et al. 1992). It has been suggested that CCS is present in the first stages of molecular cloud evolution, but it is soon destroyed (on a timescale of $\simeq 10^5$ years, Millar & Herbst 1990; Suzuki et al. 1992) after the formation of a dense core. This destruction process is induced by the core contraction (Suzuki et al. 1992) that initiates star formation. On the other hand, when the molecular cloud evolves, the physical conditions and the chemical evolution in molecular cores favor the formation of other molecules like NH_3 (Suzuki et al. 1992). For this reason the abundance ratio $[\text{NH}_3]/[\text{CCS}]$ has been considered as an indicator of the evolution of molecular cores. This time-dependent chemistry is responsible for the pronounced spatial anticorrelation observed in the emission from these two species, where ammonia tends to trace the inner regions and the CCS is found to be located outside, surrounding ammonia cores, in a clumpy distribution (Hirahara et al. 1992; Kuiper et al. 1996; Lai et al. 2003).

If this evolutionary trend (CCS more abundant in starless cores and NH_3 in more evolved, active star forming regions) is correct, any chance to use CCS as a tool to study star-formation processes will necessarily happen during the very first stages of the stellar evolution, i.e., Class 0 protostars. Interestingly, in these young protostars some of the key phenomena characteristic of the star formation (infall, disk formation and powerful mass-loss

phenomena) are especially prominent and coeval, and have their own kinematical signature, which make kinematical studies of their environment especially interesting. In this early stage of stellar evolution, the presence of water maser emission at 22 GHz is rather common. This emission is considered a good tracer of mass-loss activity in young stellar objects (YSOs) in general (Rodríguez et al. 1980; De Buizer et al. 2005), and a good indicator of the age of low-mass YSOs, since they tend to be excited preferentially in the Class 0 stage (Furuya et al. 2001).

The critical scales for these star formation processes are of the order of $\simeq 100 - 1000$ AU in the case of low mass stars ($\leq 1'' - 10''$ for nearby molecular clouds; Beltrán et al. 2001; Chen et al. 1995; Claussen et al. 1998). In order to study these phenomena with high enough resolution, it is necessary to carry out interferometric observations. This is feasible for strong maser lines, but very difficult for thermal emission (like CCS and ammonia) since it is usually weak and therefore requiring high sensitivity is needed. At wavelengths of ~ 1 cm an instrument like the Very Large Array (VLA) provides high angular resolution, but at the expense of worse atmospheric phases that blur the emission. Weak sources, in which self-calibration is not possible, would not be detected, or the quality of their maps would be poor. Nevertheless, these kinds of problems have been addressed, in the case of continuum emission, by using the cross-calibration technique. This method involves the simultaneous observation of 1 cm continuum and strong water masers, and the use of the self-calibration solutions of the latter to correct phase and amplitude errors in the weaker continuum (Torrelles et al. 1996, 1997, 1998). This technique of cross-calibration using water masers has never been applied to spectral lines. The CCS(2_1-1_0) transition at ~ 22 GHz is probably the best candidate to perform it, since it is only 110 MHz away from the H₂O ($6_{16}-5_{23}$) maser line.

A high-resolution study of the kinematics and the chemical evolution of the environment of the Class 0 source B1-IRS was carried out by de Gregorio-Monsalvo et al. (2005). In that work, CCS, ammonia, and water maser emissions at 1 cm were observed with the VLA, although cross-calibration was not possible there, since the maser was not strong enough. Three different CCS clumps were detected, whose kinematical pattern was interpreted as gas interacting with the molecular outflow that exists in the region. This interaction was not observed using other molecular tracers or with lower-resolution observations of CCS in this source (Hirota et al. 2002; Lai et al. 2003). The evidence of interaction with the outflow led de Gregorio-Monsalvo et al. (2005) to suggest the possibility that CCS abundance could be enhanced via shock-induced chemistry. Moreover, in that region a spatial anticorrelation between CCS and ammonia at scales of $\simeq 5''$ was observed for the first time, which illustrates the importance of time-dependent chemistry on small spatial scales.

In this work we present a sensitive and systematic single-dish survey of CCS emission (complemented with NH_3 observations) at 1 cm wavelength, toward low-mass star forming regions that are known to harbor water maser emission, using the NASA’s 70m antenna at Robledo de Chavela, Spain. One of our main aims is to find the best candidates to make interferometric CCS studies as the one made in B1-IRS with the VLA, but applying the cross-calibration technique for obtaining high-quality maps. Interferometric maps of CCS, ammonia and water masers would allow us to study kinematical and physical properties of star forming regions at high resolution. Another purpose of the present survey is the search for the youngest star forming regions, assuming that the presence of water masers and CCS emission are signs of youth in star forming regions. Moreover, we present a search for the relation between the CCS emission and the physical characteristics of the star forming regions of the survey, focusing on the molecular outflow properties, considering the possible association between CCS emission and the outflow suggested for B1-IRS.

This paper is structured as follows: in section §2 we describe our observations and data reduction. In section §3 we show the survey results, as well as a short description of the sources detected. We discuss the results in §4 and, finally, we summarize our conclusions in §5.

2. Observations

Observations were carried out in different periods between 2002 April and 2005 March, using the NASA’s 70-m antenna (DSS-63) at Robledo de Chavela, Spain. The total telescope time was $\simeq 50$ hours (without including calibration or pointing checks). We observed the CCS $J_N=2_1-1_0$ transition (rest frequency = 22344.033 MHz) and the $\text{NH}_3(1,1)$ inversion transition (rest frequency = 23694.496 MHz) toward a sample of star forming regions. This antenna has a 1.3 cm receiver using cooled high electron mobility transistor (HEMT) amplifiers. Calibration was performed using a noise diode. The half power beam width at these frequencies is $\simeq 40''$, and the mean beam efficiency is $\simeq 0.4$.

The sample surveyed (Table 1) consists of 40 low-mass ($L_{\text{bol}} < 100 L_{\odot}$) and intermediate-mass ($100 < L_{\text{bol}} < 10^4 L_{\odot}$) star forming regions associated with water maser emission, as a sign of youth and ongoing star formation processes. Most of the sources are low-mass star forming regions, although we have included 12 intermediate-luminosity star forming regions as a control sample, in order to test any possible relation between the CCS emission and the mass of the sources. Observations were centered at positions where water maser emission has been reported in the literature.

Most of the CCS observations were performed in frequency-switching mode. We used a 256 channel digital autocorrelator spectrometer with a bandwidth of 1 MHz, centered at the V_{LSR} of each cloud (see Table 1), which provides a velocity resolution of 0.05 km s^{-1} . Seven sources (see Table 2) were observed in position-switching mode, with a 384 channel digital autocorrelator spectrometer with a bandwidth of 2 MHz (velocity resolution of 0.07 km s^{-1}). The system temperature varied from 44 to 135 K, depending on weather conditions and elevation, with a mean system temperature of 76 K.

The ammonia observations were also made in position-switching mode, using the 384 channel digital autocorrelator spectrometer. We used a bandwidth of 16 MHz, centered at the V_{LSR} of each cloud, which provides a velocity resolution of 0.5 km s^{-1} . NGC 2071-North and AFGL 5157 were observed using a bandwidth of 4 MHz, with a velocity resolution of 0.13 km s^{-1} , but the spectra were smoothed to a final resolution of 0.5 km s^{-1} . The system temperature varied from 52 to 99 K, with a mean system temperature of 78 K.

The rms pointing accuracy was better than $10''$. The data reduction was performed using the CLASS package, which is part of the GAG software package developed at IRAM and the Observatoire de Grenoble.

3. Survey Results

In Table 2 and Table 3 we summarize the results of the survey. Out of the 40 star forming regions surveyed in the CCS (2_1-1_0) line, only 6 low-mass sources show emission, and their spectra are shown in Fig 1. We have not detected CCS emission towards any of the 12 intermediate-mass objects. On the other hand, we also observed 36 of the sources in the NH_3 (1,1) transition, of which 31 show detectable emission. We note that all sources detected in CCS are associated with ammonia emission. In order to compare our results with the work by Suzuki et al. (1992), who surveyed dark cores mostly in Taurus and Ophiucus, we will consider only the low-mass sources in our sample. We have excluded the source L260 from statistical calculations, since its noise level for CCS is significantly higher than that of the other sources. In fact, several of our CCS detections are below the upper limit given for L260 (Table 2). With this exclusion, we have a subset of 27 low-mass sources, among which we can strictly define as sources without detectable CCS emission those with $T_{\text{MB}} < 0.3 \text{ K}$ or $N_{\text{CCS}} < 2.1 \times 10^{12} \text{ cm}^{-3}$. Taking from Suzuki et al. (1992) the star forming regions (considering as such those with presence of outflows and/or IRAS sources), the detection rates obtained for CCS is 23% at 22 GHz. Since their detection limit of the CCS column density is similar to ours, we can meaningfully compare it with our detection rate of 22% for CCS. Using Fisher’s exact test, we determined that our detection rates for CCS is statistically

compatible with that of Suzuki et al. (1992), at a confidence level of 95%.¹ This compatibility is reasonable, since water maser emission (the selection criterion for our survey) is a good tracer of star formation activity (Furuya et al. 2003; Rodríguez et al. 1980).

Most of the star forming regions we surveyed have detectable ammonia emission, which suggests that ammonia survives well in the protostar phase, as indicated by the presence of water masers. Few of the regions have CCS emission, but all of these also have NH₃. Therefore, there are no regions associated with both H₂O maser and CCS emission, but without NH₃. Bearing in mind that there are many CCS-emitting clouds without any sign of harboring protostars (Benson et al. 1998; Suzuki et al. 1992), these results support the evolutionary sequence of CCS+NH₃+H₂O → NH₃+H₂O. In particular, it supports the idea that the CCS molecule is destroyed before ammonia.

3.1. Notes on the sources detected in CCS

3.1.1. L1448 Region

L1448 is a dense globule located in Perseus. This cloud contains numerous signatures of mass-loss activity (Bachiller et al. 1990, 1995b; Curiel et al. 1999) and it is an interesting environment for studying the possibility that outflows from YSOs may induce new star formation in other regions of the parental cloud. Single-dish ammonia observations reveal two peaks located at the center and at the north-east of the cloud, associated with L1448C and L1448-IRS3 respectively (Anglada et al. 1989; Bachiller et al. 1990).

L1448C (Curiel et al. 1990) is catalogued as a Class 0 source (André et al. 1993; Barsony 1994) that drives one of the most energetic and highly collimated molecular outflows ever seen in a low-mass star forming region (Bachiller et al. 1990). This outflow reveals a strong interaction with the northern material of the cloud, associated with L1448-IRS3, the brightest far-infrared source of the region.

L1448-IRS3 is known to consist of three individual Class 0 sources: a close proto-binary system [L1448N(A) and L1448N(B)], in which each component powers its own outflow, and a third source, L1448 NW (Barsony et al. 1998; Curiel et al. 1990; Terebey & Padgett 1997). Barsony et al. (1998) suggested that the outflow powered by L1448C was responsible for the formation of the proto-binary system, whose outflows may, in their turn, have produced the NW source.

¹We have used this confidence level for all the statistical tests in this paper

We detected CCS emission towards both L1448-IRS3 and L1448C. This is the first detection of emission from this molecule reported for either of them.

3.1.2. *B1-IRS*

B1-IRS (IRAS 03301+3057) is a far-infrared source located in the Perseus OB2 complex (Bachiller et al. 1990b). This source is classified as a Class 0 source (Hirano et al. 1997), and it is associated with a CO molecular outflow that displays a strong blueshifted emission (Bachiller et al. 1990b; Hirano et al. 1997).

CCS emission at 22 GHz was detected for the first time in this region by Suzuki et al. (1992). Later, Lai & Crutcher (2000) observed CCS at 33.8 GHz with the BIMA interferometer, and their maps showed a clumpy distribution surrounding B1-IRS. This clumpy distribution was confirmed with VLA CCS observations at 22 GHz (de Gregorio-Monsalvo et al. 2005). The clumps exhibit a clear velocity gradient, interpreted as gas interacting with the molecular outflow. Moreover a CCS local abundance enhancement via shock-induced chemistry was also suggested for the first time in that work. B1-IRS was the first region where a spatial anticorrelation between CCS and ammonia was detected at high angular resolution ($\simeq 5''$, de Gregorio-Monsalvo et al. 2005).

3.1.3. *NGC2071-North*

NGC2071 North is located at $20'$ north of the reflection nebula NGC2071 (Fukui et al. 1986). This region hosts a CO molecular outflow that lies near the source IRAS 05451+0037. Maps of the outflow at different angular resolution display very different geometries: a bent-U shaped outflow at $17''$ resolution, which suggests strong interaction with the ambient material (Iwata et al. 1988), and overlapping blue- and redshifted emission at $\gtrsim 50''$ resolution (Iwata et al. 1988; Goldsmith et al. 1992), which is compatible with a bipolar outflow whose axis lies very near the plane of the sky. IRAS 05451+0037 is coincident with a CS and a NH_3 peak (Goldsmith et al. 1992), and it shows the far-infrared spectrum of a T Tauri star (Iwata et al. 1988). This source was suggested to be the central engine of the molecular outflow (Iwata et al. 1988), although this is somewhat uncertain due to the complicated geometry of the outflow.

Suzuki et al. (1992) detected CCS at 45 GHz toward this source. In our survey, we report CCS emission at 22 GHz for the first time.

3.1.4. *GF9-2*

This source is located in the filamentary quiescent dark cloud GF-9 (LDN 1082), without any associated IRAS point sources or radio continuum emission (Ciardi et al. 1998; Wiesemeyer et al. 1999). It was catalogued as a transitional object between pre-stellar and proto-stellar Class 0 phase (Wiesemeyer et al. 1999), which would turn GF-9 to be the youngest source in our survey. Furuya et al. (2003) detected the presence of weak redshifted CO wing emission, and a weak H₂O maser (0.3 Jy). These authors pointed out that GF9-2 was the lowest-luminosity ($0.3 L_{\odot}$) object known to harbor H₂O masers. We have detected both CCS and ammonia emission lines toward this source for the first time.

3.1.5. *L1251A*

L1251A (IRAS 22343+7501) is located at the northern part of L1251, a small elongated cloud located in Cepheus. This source has been classified as a Class I object (Mardones et al. 1997; Nikolić et al. 2003) and appears to be powering the extended CO outflow seen in this region (Sato & Fukui 1989), as well as an optical jet (Balazs et al. 1992). Several radio continuum sources were discovered near IRAS 22343+7501 (Meehan et al. 1998). Recent VLA centimeter observations, reveal that this IRAS source may consist of two protostellar objects, with spectral indices consistent with thermal emission, and either of them could be the driving source of the CO outflow (Beltrán et al. 2001). We report CCS emission toward this source for the first time.

4. Discussion

4.1. The Lifetime of CCS in Star Forming Regions

The detection rate obtained in our survey for CCS (22% of the low-mass sources show CCS emission) is similar to the results of Suzuki et al. (1992) in star forming regions (23% detections). The low rate of detection of CCS emission in star forming regions seems to indicate that this molecule is soon destroyed after the processes associated with star formation begin. This result, together with the presence of water maser emission, allows us to roughly estimate the lifetime of CCS in low-mass star forming regions. The association of a low-mass central source with water maser emission typically lasts for one third of the duration of the embedded state (Wilking et al. 1994; Claussen et al. 1996). This embedded phase is estimated to last for $\simeq (1 - 4) \times 10^5$ yr (Wilking et al. 1989b; André & Montmerle

1994; Chen et al. 1995). Therefore, the water maser emission lasts for $\simeq (0.3 - 1.3) \times 10^5$ yr in low-mass star forming objects. If we assume that the regions of our sample are homogeneously distributed in age along the $\simeq (0.3 - 1.3) \times 10^5$ yr in which water maser emission is observed, our detection rate of 6 out of 27, would indicate that the CCS emission lasts for $\simeq (0.7 - 3) \times 10^4$ yr after star formation started.

4.2. Evolutionary stage of the SFRs associated with CCS emission

As we mentioned in the introduction, since the CCS molecule has been considered in previous works as a youth tracer of molecular cores, the star forming regions associated with this emission should contain some of the youngest YSOs. This evolutionary trend for the CCS chemistry must be valid as a general, qualitative trend when we compare large groups of molecular cores, although it may not stand in a quantitative way in the comparison of particular sources. In particular, the results of our survey do not totally agree with the first statement, since four of the sources that host CCS emission are catalogued as young Class 0 sources (GF9-2, L1448-IRS3, L1448C, B1-IRS), but L1251A and NGC2071-North are catalogued as more evolved YSOs. There are two possible explanations for these results: either the classification of the evolutionary stage of L1251A and NGC2071-North should be revised, or the particular physical conditions and processes of each source affect the production and destruction of CCS.

NGC2071-North (IRAS 05451+0037) shows a far-infrared spectrum of a T Tauri star (Iwata et al. 1988). Nevertheless, there is no optical counterpart in the POSSM prints, and no near-infrared emission in the 2MASS catalog at the position of IRAS 05451+0037, which suggests a more embedded nature of this source. The complicated geometry of the molecular outflow of the region (see section §3.1.3), makes it difficult to know reliably whether IRAS 05451+0037 is the real engine of the outflow. In order to clarify the real geometry of the outflow, the power source, and its evolutionary stage, more accurate and extended observations of CO, together with submillimeter observations, are needed. In particular, the study of possible peaks at submillimeter frequencies (typical of Class 0 objects) and the measurement of the relation L_{smm}/L_{bol} (André et al. 1993), are especially important to elucidate the possible existence of other embedded sources in the region, and to determine their evolutionary stage.

In the case of L1251A (IRAS 22343+7501), it is associated with a nebulosity visible at J, H, and K 2MASS-bands, and it is visible in POSSM plates. This source has been classified as a Class I YSO (Mardones et al. 1997; Nikolić et al. 2003). Nevertheless, Meehan et al. (1998) discovered several radio continuum sources in the region near the IRAS source,

candidates to YSOs, and the CCS emission could be associated with any of these embedded sources. In this case, higher resolution observations of CCS emission would be useful to study its association with those sources.

The second possible explanation would be to accept that, in some cases, CCS could be associated with sources in a more evolved stage. This could be the case if CCS emission depends not only on age, but also on the particular phenomena related to the star formation of each cloud. This possibility was already suggested in the high resolution CCS study of B1-IRS by de Gregorio-Monsalvo et al. (2005), who proposed that the CCS emission could be enhanced in the region where the outflow interacts with the surrounding cloud medium. The outflow interaction with fresh low-density gaseous material that exists around dense cores, could squeeze this low-density gas to the higher densities needed ($\simeq 10^5 \text{ cm}^{-3}$) to form this molecule and excite its line emission. This phenomenon could explain the detection of this molecule in stages more evolved than Class 0 sources. The possible dependence of CCS on parameters different from age is discussed in next section.

4.3. Search for dependencies of CCS emission on source and cloud parameters

The abundance ratio $[\text{NH}_3]/[\text{CCS}]$ was proposed by Suzuki et al. (1992) to be a good indicator of cloud evolution. This conclusion was based on theoretical pseudo-time-dependent calculations of the fractional abundance of CCS and NH_3 , under conditions of constant H_2 density and constant gas kinetic temperature. The variation of the fractional abundances in both molecules was explained as an effect of the evolution of the molecular clouds, with CCS more abundant in starless cores, and ammonia more abundant in regions with signs of star formation activity. Moreover, Suzuki et al. (1992) pointed out that this chemical evolutionary track was insensitive to the density of H_2 .

Nevertheless, when the column densities of both molecules (N_{NH_3} and N_{CCS}) are compared among different clouds, the proposed anticorrelation disappears (Suzuki et al. 1992). In our case, if we order the sources in which we detected CCS by their ratio of derived column densities $N_{\text{NH}_3}/N_{\text{CCS}}$, they are, from lowest to highest ratio: B1-IRS, L1448C, GF9-2, L1448-IRS3, L1251A, and NGC2071-North. If the $N_{\text{NH}_3}/N_{\text{CCS}}$ ratio were dependent on the age of cloud cores only, B1-IRS would then be the youngest source, and NGC2071-North the oldest one, but our ordering does not exactly conform to an evolutionary scheme. L1251A and NGC 2071-North have indeed been proposed to be the more evolved of these six sources, but most of the CCS non-detections seem to be younger than these two objects. On the other hand, we would expect GF9-2 to show the lowest $N_{\text{NH}_3}/N_{\text{CCS}}$ ratio, given its classification as a transitional object between prestellar and protostellar phase (Wiesemeyer et al. 1999).

These discrepancies are understandable if, as Suzuki et al. (1992) suggest, the evolutionary NH_3 -CCS anticorrelation fades out when using data from different sources.

The absence of anticorrelation among different clouds was explained by Suzuki et al. (1992) as the effect of the overlapping of individual evolutionary tracks for the chemistry of clouds with different H_2 column densities. For this reason, the relationship between column densities of CCS and ammonia may not be a good quantitative indicator of cloud evolution even assuming a common start time. This statement has also been suggested by Benson et al. (1998), who did not find statistically significant differences between star forming regions and starless cores in their CCS column density.

Furthermore, even the abundance of CCS alone has been questioned as a good quantitative tracer of cloud evolution. Lai & Crutcher (2000) suggested that the abundance of CCS is not likely to trace the age of contracting cores very sensitively. Moreover de Gregorio-Monsalvo et al. (2005) proposed that CCS abundance could be enhanced through interaction with a molecular outflow, which suggests that the local conditions and processes within each cloud could also influence the CCS emission. Being evident that CCS emission does not depend on the age of the clouds only, we have searched for other possible dependences on different parameters. To do this, we have compiled from the literature several parameters of the observed sources (luminosity, radio continuum and water maser flux densities) and of their associated molecular outflows (degree of collimation, mass, dynamical age, mechanical luminosity, kinetic energy, momentum, and momentum rate). For consistency, we obtained the outflow parameters from single-dish observations of the CO(2-1) line, when available. Otherwise, we made use of interferometric and/or data from other CO transitions.

To check whether any of these parameters of sources and outflows is related in any way with the presence of detectable CCS emission, we have tried to determine whether the parameters show different distributions in the groups of sources with and without CCS emission. The application of a Kolmogorov-Smirnov test did not find any significant difference in distribution of the source or outflow parameters.

However, when we apply the same test to the characteristics of the ammonia emission we measured, we find that the distribution of the peak ammonia intensity significantly depends on CCS detectability. Interestingly, we found no significant difference in the distribution of integrated intensity (column density) of ammonia among sources with and without CCS. In a more quantitative way, the mean peak intensity of NH_3 in the group of sources detected in CCS is 3.3 K, while that in the group of undetected sources is 2.1 K. We found that these two means are significantly different, using a T-test (and first applying a Lilliefors test to check that the involved variables follow a normal distribution, which is a prerequisite for the use of the T-test).

We have to be cautious in interpreting this result that sources with detectable CCS emission show significantly brighter NH_3 emission. We have assumed in our calculations that the filling factor of both emissions has a value of one, which is likely not to be true, at least in the case of CCS, since interferometric maps in several regions show its emission to be significantly clumpy (Velusamy et al. 1995; Lai & Crutcher 2000). Therefore, the trend we have found could be just a distance effect since, if the molecular emission does not fill the Robledo beam, sources closer to us would tend to be brighter in both CCS and NH_3 . However, we think that the observed trend of higher peak NH_3 intensity in sources with CCS is due to intrinsic characteristics of the sources, rather than to a filling factor/distance effect. The most important argument is that, if it were due to a distance bias, we would expect exactly the same trend for the NH_3 integrated intensity but, as mentioned above, we saw no significant difference for this quantity between sources with and without detectable CCS emission. On the other hand, it is not obvious that the subset of low-mass sources with CCS emission are significantly closer to us than those without emission.

A possible effect of different filling factors could be to hide real correlations between source and cloud parameters and those of the molecular line emission. However, we do not think it likely that it is showing a spurious correlation in this case. In any case, the impact of source distance on filling factors is probably not very strong, if the whole extent of the molecular emission is larger than the telescope beam. If this is the case, the filling factor of a clumpy distribution, albeit lower than 1, would not change much with distance if clumps were more or less uniformly distributed within the total spatial extent of the emission. In the case of B1–IRS, CCS and NH_3 maps show emission $\simeq 3$ times more extended than the Robledo beam ($\simeq 40''$). Ammonia maps of the sources sampled here are also typically larger than this beam (cf. Jijina et al. 1999). The lack of CCS maps in the star forming regions in which we detected this emission makes the quantification of their filling factor difficult.

The fact that we find differences in peak intensity, but not in integrated intensity can be explained if the significant decrease of NH_3 peak intensity between sources with and without detectable CCS emission is somewhat compensated by a corresponding increase in the NH_3 line width, resulting in small differences in integrated intensities. This could be interpreted in evolutionary terms, since mass-loss phenomena related to active star forming processes would increase the turbulence of the surrounding interstellar medium, thus broadening the line width as these processes progress. Therefore, younger regions would tend to show detectable CCS emission and narrower NH_3 lines. However, with our data we cannot confirm such a trend for ammonia linewidths. A Kolmogorov-Smirnov test did not find any significant difference in those linewidths between sources with and without detected CCS. It may still be possible that there is a difference, too small to be detected by the Kolmogorov-Smirnov test, but enough to blur the differences in integrated intensity between sources with or without

CCS.

It is also noticeable of interest to consider the different widths of the CCS and NH_3 lines for the 6 sources detected in the former (see Tables 2 and 3). Ammonia thermal linewidths are a factor of $\simeq 1.8$ intrinsically broader than those of CCS, due to the different masses of these molecules, but this thermal broadening alone cannot explain the observed differences. In the most extreme cases, L1448–IRS3 and GF9–2, the NH_3 line is more than 3 times broader than the CCS one. This is consistent with both lines tracing different regions of gas, with different kinematics. The narrower CCS lines would trace more quiescent gas, with less turbulence or velocity gradients. B1-IRS is the source in which both line widths are more similar, but de Gregorio-Monsalvo et al. (2005) shows that in this source, the CCS-emitting gas shows evidence of interaction with the molecular outflow, with clear velocity gradients, which makes CCS lines wider. Apart from B1-IRS, the source with the most similar line widths is L1448C, a source with an energetic molecular outflow. This could suggest that the gas traced by CCS in this region may also be significantly interacting with the molecular outflow. In this context the source GF9-2 would be the youngest source, in agreement with the transitional prestellar-protostellar classification made by Wiesemeyer et al. (1999).

We point out that these results must be considered carefully, since they are based on a small sample of regions showing CCS emission. The lack of statistically significant results for the source and outflow parameters indicates that CCS emission could be sensitive to the local temperature and density conditions of each cloud, or to filling factor/distance effects. Moreover, we must take into account that the outflow and source parameters were obtained from different instruments, and that on the other hand, the number of CCS detections is small, which would mask possible correlations. We obviously need to widen this study to include more star forming regions associated with CCS emission. Moreover, obtaining a homogeneous set of observations of outflows and source parameters (obtained with the same telescope for all sources) would be useful for improving our statistical study. While such studies will require a large amount of telescope time, it is not possible to circumvent the fact that gas and dust in star forming regions have very low surface brightness.

4.4. Prospects for future interferometric observations

There is not yet a theoretical chemical model that includes the effects of a central protostar and explains how they affect CCS and ammonia formation and destruction. High resolution observations of CCS and ammonia in star forming regions can provide the data against which such models could be tested.

Following the results obtained for the B1-IRS region (that suggest an interaction of the CCS with a molecular outflow that could enhance CCS via shocked-induced chemistry, and show for the first time a spatial anticorrelation between CCS and NH_3 at scales of $\simeq 5''$) we propose that the six detections in this survey are good candidates for high angular resolution observations, to compare with and to understand better the results obtained in B1-IRS.

All of these six sources are intrinsically interesting for detailed interferometric observations. Also, L1448C and L1448-IRS3 are especially appropriate for studying the suggested association between the CCS and the molecular outflow, since this region hosts energetic and collimated molecular outflows. Moreover, this region is a good environment for studying outflow-induced star formation. In GF9-2 it would be interesting to study the CCS and the ammonia distribution in a young object transitional between pre-stellar and protostellar Class 0 source. NGC2071-North and L1251A are good prospective sites for making high-resolution observations of CCS in regions classified as more evolved (in which very few such observations have been made), or to try to reveal whether there is a younger object driving their respective molecular outflows.

5. Conclusions

We present a single-dish survey of CCS and NH_3 emission at 1 cm, carried out with NASA’s 70m antenna at Robledo, toward a sample of low- and intermediate-mass young star forming regions that are known to harbor water maser emission. Our aim was to find the best candidates for a VLA high resolution study of the kinematical and physical properties of young Class 0 objects, to search for the youngest protostars, and to determine the relationship between CCS and NH_3 in star forming regions. Our general conclusions are the following:

- We have detected 6 low-mass sources that show CCS emission, out of a sample of 40 star forming regions associated with water maser emission. Four of these (L1448C, L1448-IRS3, GF9-2, and L1251A) had not been previously detected in any CCS transition, another one (NGC 2071-North) has been detected for the first time with the CCS line at 1 cm, while the other one (B1-IRS) had already been reported to show CCS emission in this and other transitions. All our CCS detections also show ammonia emission.
- From the CCS detection rate, and the duration of the water maser emission in low-mass star forming regions, we derive a lifetime of this molecule of $\simeq (0.7-3) \times 10^4$ yr in these regions, after star formation started.

- Three of the six sources detected in CCS are catalogued as Class 0 protostars (L1448-IRS3, L1448C and B1-IRS), one could be a transitional object between pre-stellar and protostellar Class 0 stage (GF9-2), and the last two sources (NGC2071-North and L1251A) are catalogued as more evolved, a young T Tauri and a Class I source, respectively. Since CCS is considered an early-time molecule, to explain the CCS detections in more evolved objects, we speculate with two possibilities: either the classification of NGC2071-North and L1251A should be revised, or the star formation activity and the physical properties of each cloud could influence in the production and destruction of the CCS molecules.
- We did not find any statistically significant trend that may relate the presence of CCS emission with different parameters of the molecular outflows or the central sources of these star forming regions.
- We found that the distribution and mean of the peak intensity of NH_3 in the group of sources detected in CCS are significantly different from those in the group of undetected ones, with the ammonia mean peak intensity higher in regions with CCS. However, no significant difference is found with respect to the integrated intensity of NH_3 . Stronger NH_3 peak line intensities with indistinguishable integrated intensities suggests that the lines are narrower and the emitting regions less turbulent (i.e. younger).
- The linewidths of the CCS and NH_3 lines are noticeably different, with CCS being 3 times narrower in some cases. This suggest that emission from these lines arises from gas with different kinematical properties within the telescope beam. The cases with more similar widths (B1-IRS, L1448C) may trace strong interactions between molecular outflows and the CCS-emitting gas.

JFG and IdG are partially supported by grant AYA2002-00376 of the Spanish MEC (co-funded by FEDER funds). JFG is also supported by grant AYA2005-08523-C03-03 of MEC. OS is partially supported by grant AYA2003-09499 of MEC. EJ acknowledges partial support by AYA2004-08260-C03-03 of MEC. The work by TBHK was done at the Jet Propulsion Laboratory, California Institute of Technology, under contract to the National Aeronautics and Space Administration. LFR acknowledges the support from DGAPA, UNAM, and CONACyT, Mexico. IdG acknowledges the support of a Calvo Rodés Fellowship from the Instituto Nacional de Técnica Aeroespacial (INTA). We are thankful to Jesús Calvo, Cristina García, Esther Moll, Pablo Perez, and the operators at the Madrid Deep Space Communication Complex (MDSCC) for their help before and during the observations at Robledo. This paper is based on observations taken during “host-country” allocated time at Robledo de Chavela; this time is managed by the Laboratorio de Astrofísica Espacial y Física

Fundamental (LAEFF) of INTA, under agreement with National Aeronautics and Space Administration/Ingeniería y Servicios Aeroespaciales (NASA/INSA). We would also like to thank our anonymous referee, whose valuable comments have greatly improved the quality of this paper.

REFERENCES

- André, P., & Montmerle, T. 1994, *ApJ*, 420, 837
- André, P., Ward-Thompson, D., & Barsony, M. 1993, *ApJ*, 406, 122
- André, P., Ward-Thompson, D., & Barsony, M. 2000, *Protostars and Planets IV*, 59
- Anglada, G., Estalella, R., Pastor, J., Rodríguez, L. F., & Haschick, A. D. 1996, *ApJ*, 463, 205
- Anglada, G., Rodríguez, L. F., Torrelles, J. M., Estalella, R., Ho, P. T. P., Cantó, J., López, R., & Verdes-Montenegro, L. 1989, *ApJ*, 341, 208
- Bachiller, R., Fuente, A., & Tafalla, M. 1995, *ApJ*, 445, L51
- Bachiller, R., Guilloteau, S., Dutrey, A., Planesas, P., & Martín-Pintado, J. 1995b, *A&A*, 299, 857
- Bachiller, R., Martín-Pintado, J., Tafalla, M., Cernicharo, J., & Lazareff, B. 1990, *A&A*, 231, 174
- Bachiller, R., del Río Álvarez, S., & Menten, K. M. 1990b, *A&A*, 236, 461
- Balazs, L. G., Eisloffel, J., Holl, A., Kelemen, J., & Kun, M. 1992, *A&A*, 255, 281
- Barsony, M. 1994, *ASP Conf. Ser.* 65: *Clouds, Cores, and Low Mass Stars*, 197
- Barsony, M., Ward-Thompson, D., André, P., & O’Linger, J. 1998, *ApJ*, 509, 733
- Beichman, C. A., Myers, P. C., Emerson, J. P., Harris, S., Mathieu, R., Benson, P. J., & Jennings, R. E. 1986, *ApJ*, 307, 337
- Beltrán, M. T., Estalella, R., Anglada, G., Rodríguez, L. F., & Torrelles, J. M. 2001, *AJ*, 121, 1556 *ApJ*, 573, 246
- Benson, P. J., Caselli, P., & Myers, P. C. 1998, *ApJ*, 506, 743

- Benson, P. J., & Myers, P. C. 1989, *ApJS*, 71, 89
- Bontemps, S., André, P., Terebey, S., & Cabrit, S. 1996, *A&A*, 311, 858
- Brand, J., et al. 1994, *A&AS*, 103, 541
- Cabrit, S., & Bertout, C. 1992, *A&A*, 261, 274
- Cesaroni, R., Palagi, F., Felli, M., Catarzi, M., Comoretto, G., di Francos, Giovanardi, C., & Palla, F. 1988, *A&AS*, 76, 445
- Chen, H., Myers, P. C., Ladd, E. F., & Wood, D. O. S. 1995, *ApJ*, 445, 377
- Ciardi, D. R., Woodward, C. E., Clemens, D. P., Harker, D. E., & Rudy, R. J. 1998, *AJ*, 116, 349
- Claussen, M. J., Wilking, B. A., Benson, P. J., Wootten, A., Myers, P. C., & Terebey, S. 1996, *ApJS*, 106, 111
- Claussen, M. J., Marvel, K. B., Wootten, A., & Wilking, B. A. 1998, *ApJ*, 507, L79
- Clemens, D. P., & Barvainis, R. 1988, *ApJS*, 68, 257
- Codella, C., & Felli, M. 1995, *A&A*, 302, 521
- Codella, C., & Muders, D. 1997, *MNRAS*, 291, 337
- Comoretto, G., Palagi, F., Cesaroni, R., Felli, M., Bettarini, A., Catarzi, M., Curioni, G. P., Curioni, P., di Franco, S., Giovanardi, C., Massi, M., Palla, F., Panella, D., Rossi, E., Speroni, N., Tofani, G. 1990, *A&AS*, 84, 179
- Curiel, S., Raymond, J. C., Moran, J. M., Rodríguez, L. F., & Cantó, J. 1990, *ApJ*, 365, L85
- Curiel, S., Torrelles, J. M., Rodríguez, L. F., Gómez, J. F., & Anglada, G. 1999, *ApJ*, 527, 310
- Davidson, J. A. 1987, *ApJ*, 315, 602
- Davis, C. J., & Eisloffel, J. 1995, *A&A*, 300, 851
- de Gregorio-Monsalvo, I., Chandler, C. J., Gómez, J. F., Kuiper, T. B. H., Torrelles, J. M., & Anglada, G. 2005, *ApJ*, 628, 789
- De Buizer, J. M., Radomski, J. T., Telesco, C. M., & Piña, R. K. 2005, *ApJS*, 156, 179

- Edwards, S., & Snell, R. L. 1983, *ApJ*, 270, 605
- Eiroa, C., Torrelles, J. M., Gómez, J. F., Sakamoto, S., Hasegawa, T., Kawabe, R., Hayashi, M., & Casali, M. M. 1992, *PASJ*, 44, 155
- Evans, N. J., Levreault, R. M., & Harvey, P. M. 1986, *ApJ*, 301, 894
- Felli, M., Palagi, F., & Tofani, G. 1992, *A&A*, 255, 293
- Froebrich, D. 2005, *ApJS*, 156, 169
- Fukui, Y., Sugitani, K., Takaba, H., Iwata, T., Mizuno, A., Ogawa, H., & Kawabata, K. 1986, *ApJ*, 311, L85
- Furuya, R. S., Kitamura, Y., Wootten, H. A., Claussen, M. J., & Kawabe, R. 2001, *ApJ*, 559, L143
- Furuya, R. S., Kitamura, Y., Wootten, A., Claussen, M. J., & Kawabe, R. 2003, *ApJS*, 144, 71
- Gibb, A. G., & Little, L. T. 2000, *MNRAS*, 313, 663
- Goldsmith, P. F., Margulis, M., Snell, R. L., & Fukui, Y. 1992, *ApJ*, 385, 522
- Goldsmith, P. F., Snell, R. L., Hemeon-Heyer, M., & Langer, W. D. 1984, *ApJ*, 286, 599
- Goodman, A. A., Benson, P. J., Fuller, G. A., & Myers, P. C. 1993, *ApJ*, 406, 528
- Graf, U. U., Eckart, A., Genzel, R., Harris, A. I., Poglitsch, A., Russell, A. P. G., & Stutzki, J. 1993, *ApJ*, 405, 249
- Harju, J., Walmsley, C. M., & Wouterloot, J. G. A. 1993, *A&AS*, 98, 51
- Harvey, P. M., Campbell, M. F., Hoffmann, W. F., Thronson, H. A., & Gatley, I. 1979, *ApJ*, 229, 990
- Harvey, P. M., Joy, M., Lester, D. F., & Wilking, B. A. 1986, *ApJ*, 301, 346
- Henkel, C., Guesten, R., & Haschick, A. D. 1986, *A&A*, 165, 197
- Henning, T., Cesaroni, R., Walmsley, M., & Pfau, W. 1992, *A&AS*, 93, 525
- Heyer, M. H., Snell, R. L., Goldsmith, P. F., & Myers, P. C. 1987, *ApJ*, 321, 370
- Hirahara, Y., Suzuki, H., Yamamoto, S., Kawaguchi, K., Kaifu, N., Ohishi, M., Takano, S., Ishikawa, S., Masuda, A. 1992, *ApJ*, 394, 539

- Hirano, N., Kameya, O., Mikami, H., Saito, S., Umemoto, T., & Yamamoto, S. 1997, *ApJ*, 478, 631
- Hirota, T., Ito, T., & Yamamoto, S. 2002, *ApJ*, 565, 359
- Ho, P. T. P. & Townes, C. H. 1983, *ARA&A*, 21, 239
- Hurt, R. L., & Barsony, M. 1996, *ApJ*, 460, L45
- Iwata, T., Fukui, Y., & Ogawa, H. 1988, *ApJ*, 325, 372
- Jennings, R. E., Cameron, D. H. M., Cudlip, W., & Hirst, C. J. 1987, *MNRAS*, 226, 461
- Jijina, J., Myers, P. C., & Adams, F. C. 1999, *ApJS*, 125, 161
- Kuiper, T. B. H., Langer, W. D., & Velusamy, T. 1996, *ApJ*, 468, 761
- Ladd, E. F., & Hodapp, K.-W. 1997, *ApJ*, 474, 749
- Lai, S. & Crutcher, R. M. 2000, *ApJS*, 128, 271
- Lai, S., Velusamy, T., Langer, W. D., & Kuiper, T. B. H. 2003, *AJ*, 126, 311
- Langer, W. D., Castets, A., & Lefloch, B. 1996, *ApJ*, 471, L111
- Lorenzetti, D.; Giannini, T.; Nisini, B.; Benedettini, M.; Creech-Eakman, M.; Blake, G. A.; van Dishoeck, E. F.; Cohen, M.; Liseau, R.; Molinari, S.; Pezzuto, S.; Saraceno, P.; Smith, H. A.; Spinoglio, L.; White, G. J. 2000, *A&A*, 357, 1035
- Mardones, D., Myers, P. C., Tafalla, M., Wilner, D. J., Bachiller, R., & Garay, G. 1997, *ApJ*, 489, 719
- Margulis, M., Lada, C. J., & Young, E. T. 1989, *ApJ*, 345, 906
- Meehan, L. S. G., Wilking, B. A., Claussen, M. J., Mundy, L. G., & Wootten, A. 1998, *AJ*, 115, 1599
- Millar, T. J. & Herbst, E. 1990, *A&A*, 231, 466
- Mikami, H., Umemoto, T., Yamamoto, S., & Saito, S. 1992, *ApJ*, 392, L87
- Molinari, S., Brand, J., Cesaroni, R., & Palla, F. 2000, *A&A*, 355, 617
- Momose, M., Ohashi, N., Kawabe, R., Hayashi, M., & Nakano, T. 1996, *ApJ*, 470, 1001

- Myers, P. C., Fuller, G. A., Mathieu, R. D., Beichman, C. A., Benson, P. J., Schild, R. E., & Emerson, J. P. 1987, *ApJ*, 319, 340
- Nikolić, S., Johansson, L. E. B., & Harju, J. 2003, *A&A*, 409, 941
- Pastor, J., Buj, J., Estalella, R., López, R., Anglada, G., & Planesas, P. 1991, *A&A*, 252, 320
- Persi, P., Palagi, F., & Felli, M. 1994, *A&A*, 291, 577
- Rodríguez, L. F., Moran, J. M., Gottlieb, E. W., & Ho, P. T. P. 1980, *ApJ*, 235, 845
- Richer, J. S., Padman, R., Ward-Thompson, D., Hills, R. E., & Harris, A. I. 1993, *MNRAS*, 262, 839
- Saito, S., Kawaguchi, K., Yamamoto, S., Ohishi, M., Suzuki, H., & Kaifu, N. 1987, *ApJ*, 317, L115
- Sato, F., & Fukui, Y. 1989, *ApJ*, 343, 773
- Sato, F., Mizuno, A., Nagahama, T., Onishi, T., Yonekura, Y., & Fukui, Y. 1994, *ApJ*, 435, 279
- Snell, R. L., Huang, Y.-L., Dickman, R. L., & Claussen, M. J. 1988, *ApJ*, 325, 853
- Stanke, T., McCaughrean, M. J., & Zinnecker, H. 2000, *A&A*, 355, 639
- Sugitani, K., Fukui, Y., Mizuni, A., & Ohashi, N. 1989, *ApJ*, 342, L87
- Suzuki, H., Yamamoto, S., Ohishi, M., Kaifu, N., Ishikawa, S., Hirahara, Y., & Takano, S. 1992, *ApJ*, 392, 551
- Tafalla, M., Bachiller, R., & Martín-Pintado, J. 1993, *ApJ*, 403, 175
- Terebey, S. & Padgett, D. L. 1997, *IAU Symp. 182: Herbig-Haro Flows and the Birth of Stars*, 182, 507
- Tofani, G., Felli, M., Taylor, G. B., & Hunter, T. R. 1995, *A&AS*, 112, 299
- Torrelles, J. M., Gómez, J. F., Ho, P. T. P., Anglada, G., Rodríguez, L. F., & Cantó, J. 1993, *ApJ*, 417, 655
- Torrelles, J. M., Gómez, J. F., Rodríguez, L. F., Curiel, S., Anglada, G., & Ho, P. T. P. 1998, *ApJ*, 505, 756

- Torrelles, J. M., Gómez, J. F., Rodríguez, L. F., Curiel, S., Ho, P. T. P., & Garay, G. 1996, *ApJ*, 457, L107
- Torrelles, J. M., Gómez, J. F., Rodríguez, L. F., Ho, P. T. P., Curiel, S., & Vázquez, R. 1997, *ApJ*, 489, 744
- Velusamy, T., Kuiper, T. B. H., & Langer, W. D. 1995, *ApJ*, 451, L75
- Wang, Y., Evans, N. J., Zhou, S., & Clemens, D. P. 1995, *ApJ*, 454, 217
- Wiesemeyer, H., Cox, P., Gusten, R., & Zylka, R. 1999, *ESA SP-427: The Universe as Seen by ISO*, 533
- Wilking, B. A., Blackwell, J. H., Mundy, L. G., & Howe, J. E. 1989a, *ApJ*, 345, 257
- Wilking, B. A., Claussen, M. J., Benson, P. J., Myers, P. C., Terebey, S., & Wootten, A. 1994, *ApJ*, 431, L119
- Wilking, B. A., Claussen, M. J., Benson, P. J., Myers, P. C., Terebey, S., & Wootten, A. 1994b, *ASP Conf. Ser.* 65: *Clouds, Cores, and Low Mass Stars*, 65, 299
- Wilking, B. A., Lada, C. J., & Young, E. T. 1989b, *ApJ*, 340, 823
- Wolkovitch, D., Langer, W. D., Goldsmith, P. F., & Heyer, M. 1997, *ApJ*, 477, 241
- Wouterloot, J. G. A., & Brand, J. 1989, *A&AS*, 80, 149
- Wouterloot, J. G. A., Brand, J., & Fiegle, K. 1993, *A&AS*, 98, 589
- Wouterloot, J. G. A., Walmsley, C. M., & Henkel, C. 1988, *A&A*, 203, 367
- Wu, Y., Wei, Y., Zhao, M., Shi, Y., Yu, W., Qin, S., & Huang, M. 2004, *A&A*, 426, 503
- Wu, Y., Wu, J., & Wang, J. 2001, *A&A*, 380, 665
- Yang, J., Ohashi, N., & Fukui, Y. 1995, *ApJ*, 455, 175
- Zinnecker, H., Bastien, P., Arcoragi, J.-P., & Yorke, H. W. 1992, *A&A*, 265, 726

Table 1. Observed sources

Source	Alternative name	Right Ascension ^a (J2000)	Declination ^a (J2000)	$V_{\text{LSR}}^{\text{b}}$ (km s ⁻¹)	$L_{\text{bol}}^{\text{c}}$ (L_{\odot})	D^{d} (pc)	References ^e
L1287 ^f	IRAS 00338+6312	00 36 47.5	+63 29 02	-18.0	1000	850	11,67,42
L1448-IRS3	IRAS 03225+3034	03 25 36.4	+30 45 20	4.5	10	300	12,5,8
L1448C	LDN 1448-mm	03 25 38.7	+30 44 05	4.5	9	300	12,5,8
RNO 15 FIR	IRAS 03245+3002	03 27 39.0	+30 12 59	5.2	16	350	12,63,60
IRAS 2A	IRAS 03258+3104	03 28 55.4	+31 14 35	7.0	43	350	24,41,23
HH 6	IRAS 7	03 29 11.2	+31 18 31	7.0	18	350	33,19,39
B1-IRS	IRAS 03301+3057	03 33 16.3	+31 07 51	6.3	2.8	350	24,36
T TAU-South	IRAS 04190+1924	04 21 59.4	+19 32 06	8.2	10	160	12,46,10
L1534B	IRAS 04361+2547	04 39 13.9	+25 53 21	6.2	3.8	140	12,35,8
L1641-North ^f	IRAS 05338-0624	05 36 18.7	-06 22 09	7.4	120	500	12,61,22
HH 1	IRAS 05339-0647	05 36 19.1	-06 45 01	9.3	50	500	16,57,32
AFGL 5157 ^f	IRAS 05345+3157	05 37 47.8	+31 59 24	-18.0	5000	1800	34,48,52
Haro4-255	IRAS 05369-0728	05 39 22.3	-07 26 45	4.8	13	480	12,2,21
L1641-S3	IRAS 05375-0731	05 39 56.0	-07 30 18	5.1	70	450	12,61,53
NGC 2024 FIR 5	Orion B	05 41 44.5	-01 55 43	11.0	$\gtrsim 10$	450	24,29,1
HH 212	IRAS 05413-0104	05 43 51.1	-01 03 01	1.7	14	500	12,30,68
B35A	IRAS 05417+0907	05 44 29.8	+09 08 54	11.8	15	460	12,7,6
HH 19-27	NGC 2068 H ₂ O maser	05 46 31.2	-00 02 35	9.9	1.7	400	3,48,25
NGC 2071 ^f	IRAS 05445+0020	05 47 04.8	+00 21 43	9.4	750	500	56,64,31
NGC 2071-North	IRAS 05451+0037	05 47 42.3	+00 38 40	9.0	40	500	12,64,38
IRAS 06291+0421 ^f		06 31 48.1	+04 19 31	13.7	1882	1600	9,66,65
NGC 2264 IRS ^f	IRAS 06384+0932	06 41 10.3	+09 29 19	8.7	2300	800	22,64,43
IRAS 06584-0852 ^f		07 00 51.5	-08 56 29	40.5	5670	4480	49,66,45
CB 54	IRAS 07020-1618	07 04 21.2	-16 23 15	19.5	55	600	27,13,58
L260	IRAS 16442-0930	16 46 58.6	-09 35 23	3.5	0.97	160	22,28,47
IRAS 18265+0028 ^f		18 29 05.8	+00 30 36	5.3	347	440	14,49
Serpens FIRS 1	IRAS 18273+0113	18 29 49.8	+01 15 21	8.0	46	310	12,20,37
LDN 723-mm	IRAS 19156+1906	19 17 53.9	+19 12 25	10.5	3	300	24,26,17
IRAS 20050+2720 ^f	IRAS 20050+2720 MMS 1	20 07 06.7	+27 28 53	6.0	260	700	9,4,61
S106 FIR ^f	IRAS 20255+3712	20 27 25.5	+37 22 49	-1.0	<1000	600	24,63,50
L1157-mm	IRAS 20386+6751	20 39 06.5	+68 02 13	2.7	11	440	12,44,18
GF9-2		20 51 30.1	+60 18 39	-2.7	0.3	200	24,59
B361	IRAS 21106+4712	21 12 26.1	+47 24 24	2.7	4.7	350	12,28,6
CB 232	IRAS 21352+4307	21 37 11.3	+43 20 36	12.6	3.9	350	27,13,15
IC 1369N ^f	IRAS 21391+5802	21 40 42.4	+58 16 10	0.2	500	750	9,62,54
L1204A ^f	IRAS 22198+6336	22 21 27.6	+63 51 42	-10.5	367	900	24,63,22
L1204B	IRAS 22199+6322	22 21 33.3	+63 37 21	-10.3	52	900	14,55,22
L1251A	IRAS 22343+7501	22 35 24.3	+75 17 06	-4.0	27	300	12,28,51
L1251B	IRAS 22376+7455	22 38 47.1	+75 11 29	-4.0	14	300	12,51
Cepheus E	IRAS 23011+6126	23 03 13.1	+61 42 26	-10.4	50	730	24,64,40

^aObserved position, coincident with reported water maser position. Units of right ascension are hours, minutes, and seconds. Units of declination are degrees, arcminutes, and arcseconds

^bVelocity of the cloud with respect to the local standard of rest

^cBolometric luminosity of the source

^dDistance to the source

^eREFERENCES:(1)André et al. 2000, (2)Anglada et al. 1989, (3)Anglada et al. 1996, (4)Bachiller et al. 1995, (5)Bachiller et al. 1990, (6)Beichman et al. 1986, (7)Benson & Myers 1989, (8)Bontemps et al. 1996, (9)Brand et al. 1994, (10)Cabrit & Bertout 1992, (11)Cesaroni et al. 1988, (12)Claussen et al. 1996, (13)Clemens & Barvainis 1988, (14)Codella & Felli 1995, (15)Codella & Muders 1997, (16)Comoretto et al. 1990, (17)Davidson 1987, (18)Davis & Eisloffel 1995, (19)Edwards & Snell 1983, (20)Eiroa et al. 1992, (21)Evans et al. 1986, (22)Felli et al. 1992, (23)Froebrich 2005, (24)Furuya et al. 2003, (25)Gibb & Little 2000, (26)Goldsmith et al. 1984, (27)Gómez et al. in preparation, (28)Goodman et al. 1993, (29)Graf et al. 1993, (30)Harju et al. 1993, (31)Harvey et al. 1979, (32)Harvey et al. 1986, (33)Henkel et al. 1986, (34)Henning et al. 1992, (35)Heyer et al. 1987, (36)Hirano et al. 1997, (37)Hurt & Barsony 1996, (38)Iwata et al. 1988, (39)Jennings et al. 1987, (40)Ladd & Hodapp 1997, (41)Langer et al. 1996, (42)Lorenzetti et al. 2000, (43)Margulis et al. 1989, (44)Mikami et al. 1992, (45)Molinari et al. 2000, (46)Momose et al. 1996, (47)Myers et al. 1987, (48)Pastor et al. 1991, (49)Persi et al. 1994, (50)Richer et al. 1993, (51)Sato et al. 1994, (52)Snell et al. 1988, (53)Stanke et al. 2000, (54)Sugitani et al. 1989, (55)Tafalla et al. 1993, (56)Tofani et al. 1995, (57)Torrelles et al. 1993, (58)Wang et al. 1995, (59)Wiesemeyer et al. 1999, (60)Wilking et al. 1994b, (61)Wilking et al. 1989a, (62)Wouterloot & Brand 1989, (63)Wouterloot et al. 1993, (64)Wouterloot et al. 1988, (65)Wu et al. 2004, (66)Wu et al. 2001, (67)Yang et al. 1995, (68)Zinnecker et al. 1992

^fIntermediate-luminosity ($L_{bol} > 100 L_{\odot}$) sources.

Table 2. CCS (2_1-1_0) line parameters ^a

Source	T_{MB}^{b} (K)	$V_{\text{LSR}}^{\text{c}}$ (km s ⁻¹)	Δv^{c} (km s ⁻¹)	$\int T_{\text{MB}} dv^{\text{d}}$ (K km s ⁻¹)	$N_{\text{CCS}}^{\text{e}}$ (10 ¹² cm ⁻²)
L1287	<0.3	<0.07	<1.9
L1448–IRS3	0.32±0.11	4.68±0.05	0.36±0.11	0.09±0.03	2.4±0.8
L1448C	0.46±0.07	4.65±0.03	0.58±0.07	0.305±0.024	8.1±0.6
RNO 15 FIR	<0.15	<0.03	<0.8
IRAS 2A	<0.21	<0.05	<1.3
HH 6	<0.24	<0.05	<1.3
B1–IRS	0.70±0.13	6.72±0.04	0.89±0.10	0.57±0.05	15.1±1.3
T TAU–South	<0.22	<0.05	<1.3
L1534B	<0.20	<0.04	<1.1
L1641–North ^f	<0.20	<0.05	<1.3
HH 1 ^f	<0.24	<0.06	<1.6
AFGL 5157	<0.3	<0.07	<1.9
Haro4–255	<0.3	<0.07	<1.9
L1641–S3	<0.22	<0.05	<1.3
NGC 2024 FIR 5	<0.20	<0.04	<1.1
HH 212	<0.3	<0.07	<1.9
B35A	<0.23	<0.05	<1.3
HH 19–27	<0.3	<0.07	<1.9
NGC 2071 ^f	<0.24	<0.06	<1.6
NGC 2071–North	0.41±0.12	8.54±0.04	0.38±0.08	0.14±0.03	3.7±0.8
IRAS 06291+0421	<0.3	<0.07	<1.9
NGC 2264 IRS	<0.20	<0.04	<1.1
IRAS 06584–0852	<0.23	<0.05	<1.3
CB 54	<0.22	<0.05	<1.3
L260	<0.5	<0.11	<3
IRAS 18265+0028	<0.20	<0.04	<1.1
Serpens FIRS 1	<0.20	<0.04	<1.1
LDN 723–mm	<0.3	<0.07	<1.9
IRAS 20050+2720	<0.3	<0.07	<1.9
S106 FIR	<0.15	<0.03	<0.8
L1157–mm ^f	<0.18	<0.05	<1.3
GF9–2 ^f	0.90±0.16	–2.415±0.022	0.24±0.05	0.25±0.05	6.6±1.3
B361	<0.16	<0.04	<1.1
CB 232	<0.24	<0.05	<1.3
IC 1369N	<0.3	<0.07	<1.9
L1204A	<0.24	<0.05	<1.3
L1204B	<0.3	<0.07	<1.9
L1251A ^f	0.59±0.11	–4.91±0.04	0.47±0.09	0.28±0.04	7.4±1.1
L1251B ^f	<0.3	<0.08	<2.1
Cepheus E	<0.3	<0.07	<1.9

^aUncertainties in this table are 2σ for detections. For nondetections, upper limits are 3σ .

^bMain beam brightness temperature.

^cCentral V_{LSR} and line width obtained from a Gaussian fit to the CCS line. Uncertainties represent the error in the Gaussian fit.

^dIntegrated intensity. Upper limits were calculated assuming a width equal to the mean value of

velocity width for detections ($\Delta v \simeq 0.5 \text{ km s}^{-1}$).

^eCCS column density obtained from $N_{\text{mol}} = \frac{8\pi\nu^3}{c^3 g_j A_{ji}} \frac{Q(T_{\text{rot}}) \int T_M B dv}{[B_\nu(T_{\text{ex}}) - B_\nu(T_{\text{bg}})]} \frac{\exp(E_j/kT_{\text{rot}})}{\exp(h\nu/kT_{\text{ex}}) - 1}$ (optically thin approximation), ν is the frequency of the transition, Q is the partition function, E_j is the energy of the upper state (1.61 K; Wolkovitch et al. 1997), T_{rot} is the rotational temperature, g_j is the statistical weight of the upper rotational level. A_{ji} is the Einstein coefficient for the CCS(2₁-1₀) transition ($4.33 \times 10^{-7} \text{ s}^{-1}$; Wolkovitch et al. 1997), $B(T)$ is the intensity of black-body radiation at temperature T , and T_{ex} is the excitation temperature. Since we only observed one CCS transition, we could not obtain a reliable estimate of T_{ex} and T_{rot} ; therefore, we assumed $T_{\text{rot}} = T_{\text{ex}} = 5 \text{ K}$, the mean value assigned by Suzuki et al. (1992) for a large sample of young sources. We assumed these values even for the intermediate-mass sources, since, for instance, an increase of 4 K in both T_{ex} and T_{rot} causes a change in the CCS column density of only $\simeq 45\%$.

^fSources observed using the 384 channel spectrometer, with a velocity resolution of 0.07 km s^{-1} . These sources were smoothed to a final velocity resolution of $\simeq 0.14 \text{ km s}^{-1}$. The rest of CCS targets (observed with the 256 channel spectrometer with a velocity resolution of 0.05 km s^{-1}) were smoothed to a resolution of 0.10 km s^{-1} .

Table 3. NH₃(1,1) line parameters ^a

Source	T _{MB} ^b (K)	V _{LSR} ^c (km s ⁻¹)	Δv ^c (km s ⁻¹)	∫ T _{MB} dv ^d (K km s ⁻¹)	N _{NH3} ^e (10 ¹⁵ cm ⁻²)
L1287	3.9±0.3	-17.73±0.12	2.2±0.3	9.3±0.5	2.76±0.15
L1448–IRS3	5.7±0.3	4.22±0.07	1.17±0.16	7.7±0.4	1.52±0.08
L1448C	4.97±0.24	4.60±0.03	1.28±0.14	6.8±0.3	1.00±0.04
RNO 15 FIR	2.73±0.21	4.50±0.06	1.00±0.14	3.2±0.3	1.33±0.12
IRAS 2A	1.70±0.13	7.27±0.09	1.69±0.19	3.15±0.17	5.0±0.3
HH 6	1.8±0.3	8.27±0.10	1.1±0.3	2.3±0.5	2.4±0.5
B1–IRS	4.04±0.24	5.95±0.06	1.06±0.14	5.2±0.4	1.79±0.14
T TAU–South	<0.3	<0.3	<0.09
L1534B	<0.5	<0.4	<0.12
L1641–North	3.68±0.21	7.11±0.04	1.27±0.18	5.2±0.3	1.25±0.07
HH 1	0.83±0.22	9.02±0.07	2.1±0.5	1.8±0.3	27±5
AFGL 5157 ^f	<0.3	<0.3	<0.09
Haro4–255	1.7±0.3	4.44±0.10	1.07±0.24	2.0±0.4	3.2±0.7
L1641–S3	2.6±0.4	5.28±0.12	1.5±0.3	4.0±0.5	3.4±0.4
NGC 2024 FIR 5	1.94±0.22	11.12±0.13	2.5±0.3	4.8±0.4	1.17±0.10
HH 212	1.16±0.21	1.65±0.06	0.8±0.3	1.4±0.3	11.2±2.4
B35A	2.25±0.21	11.88±0.06	1.04±0.17	2.7±0.3	2.05±0.22
HH 19–27	1.57±0.13	10.24±0.06	1.12±0.16	2.34±0.22	4.4±0.4
NGC 2071	3.12±0.24	8.94±0.07	1.44±0.18	5.0±0.4	0.41±0.03
NGC 2071–North ^f	1.02±0.07	8.37±0.11	1.03±0.26	0.94±0.13	4.5±0.6
IRAS 06291+0421	<0.3	<0.3	<0.09
NGC 2264 IRS	5.09±0.23	8.22±0.12	2.7±0.3	13.2±0.4	1.42±0.04
IRAS 06584–0852	<0.3	<0.3	<0.09
CB 54	0.98±0.13	19.55±0.09	1.3±0.3	1.40±0.21	0.140±0.021
LDN 723–mm	1.63±0.18	10.89±0.06	0.88±0.15	1.63±0.23	0.67±0.09
IRAS 20050+2720	2.27±0.11	5.88±0.11	2.5±0.3	6.19±0.20	3.80±0.12
S106 FIR	0.78±0.19	-1.57±0.16	1.4±0.4	1.0±0.3	0.56±0.18
L1157–mm	2.24±0.17	2.64±0.06	0.84±0.12	2.00±0.21	1.12±0.12
GF9–2	3.32±0.18	-2.49±0.06	0.80±0.11	2.71±0.22	1.36±0.11
B361	2.3±0.3	2.76±0.10	1.5±0.3	3.5±0.4	0.28±0.03
CB 232	1.00±0.11	12.39±0.07	0.99±0.15	1.10±0.15	2.7±0.4
IC 1369N	1.79±0.21	0.50±0.11	2.1±0.3	4.2±0.4	1.79±0.17
L1204A	1.78±0.19	-11.00±0.09	1.44±0.19	2.9±0.3	4.4±0.5
L1204B	1.49±0.22	-10.56±0.10	1.39±0.22	2.2±0.3	2.9±0.4
L1251A	0.75±0.13	-5.33±0.12	1.4±0.3	1.11±0.18	6.5±1.1
Cepheus E	1.03±0.21	-11.05±0.11	1.01±0.24	1.0±0.3	2.2±0.7

^aUncertainties in this table are 2σ for detections. For nondetections, upper limits are 3σ.

^bMain beam brightness temperature of the main hyperfine component.

^cCentral V_{LSR} and line width obtained from a Gaussian fit to the main line of the NH₃(1,1) transition. Uncertainties represent the error in the Gaussian fit.

^dIntegrated intensity of the main hyperfine component. Upper limits were calculated assuming a width equal to the mean value of velocity width for detections (Δv ≈ 1.4 km s⁻¹).

^eColumn density obtained from $N_{\text{mol}} = \frac{16[1+\exp(h\nu/kT_{\text{ex}})]\pi\nu^3}{c^3 g_j A_{ji}} \frac{Q(T_{\text{rot}}) \int T_M B dv}{[B_\nu(T_{\text{ex}}) - B_\nu(T_{\text{bg}})] \exp(h\nu/kT_{\text{ex}}) - 1} \frac{\exp(E_j/kT_{\text{rot}})}{\exp(h\nu/kT_{\text{ex}}) - 1}$ (optically thin approximation). E_j is the energy of the $J, K = 1, 1$ rotational level (23.4 K);

Ho & Townes 1983), g_j is the statistical weight of the upper sublevel involved in the inversion transition, A_{ji} is the Einstein coefficient of the $\text{NH}_3(1,1)$ transition ($1.67 \times 10^{-7} \text{s}^{-1}$; Ho & Townes 1983). We calculated the optical depth and the excitation temperature from the relationship between hyperfine components for each source. When no satellite hyperfine line was detected, we adopted $T_{\text{ex}} = 7.8 \text{ K}$, the mean T_{ex} of all the sources. We assumed $T_{\text{rot}} = T_{\text{ex}}$.

^fSources observed with a velocity resolution of 0.13 km s^{-1} . These sources were smoothed to a final velocity resolution of 0.5 km s^{-1} . The rest of the ammonia targets were observed with a velocity resolution of 0.5 km s^{-1} .

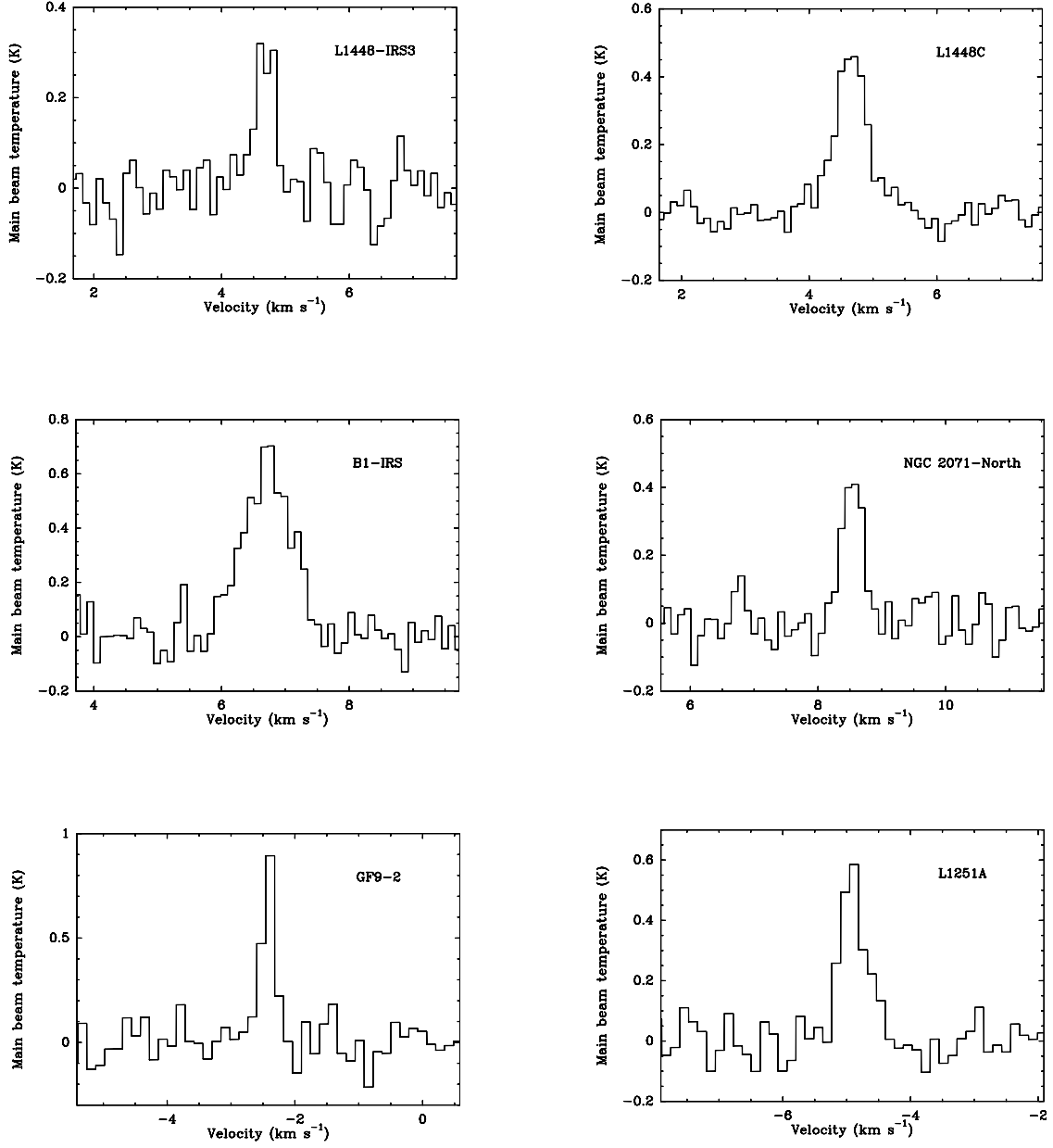


Fig. 1.— Spectra of CCS(2_1-1_0) transition detected with the Robledo 70m antenna.